Design and Control of a Force-Reflecting Teleoperation System with Magnetically Levitated Master and Wrist

S.E. Salcudean, N.M. Wong and R. L. Hollis

Abstract— **A new approach to the design of teleoperation systems is presented. It is proposed that the teleoperation slave be a coarse-fine manipulator with a fine-motion wrist identical to the teleoperation master. By using a combination of position and rate control, such a system would require only small operator hand motions but would provide low mechanical impedance, high motion resolution and force feedback over a substantial volume.**
A new teleoperation system, consisting of a conventional manipulator and two identical magnetically levitated wrists has been developed using this approach and is described in this paper. Aspects of mechanical, system and computational design are discussed.
It is shown that the best way to position the slave is by decoupling position and rate control, with the conventional robot controlled in rate mode and its wrist in position mode. Kinesthetic feedback is achieved through wrist-level coordinated force control. Transparency is improved through feedforward of sensed hand forces to the master and environment forces to the slave. To maintain stability, the amount of damping in the system is controlled by the sensed environment forces. Experimental results demonstrating excellent performance are presented.

I. Introduction

Teleoperation is emerging as a powerful way of extending the human sensing and manipulation abilities not only to remote and sometimes hazardous locations [1], [2], but also across barriers of scale [3], [4], [5], [6], [7]. Teleoperation may also emerge as a useful tool for robot programming, with force-feedback devices replacing conventional teaching pendants for "teaching and playback" of assembly sequences without the complicated modelling of the dynamics of mating parts.

The teleoperation systems reported to date suffer from the same drawbacks as conventional robot technology, which, due to constraints on workspace, payload and cost, has produced serial mechanisms with high mechanical impedance and friction, low position and force frequency responses, and poor ability to exert accurate forces. These limitations affect the achievable "transparency" of teleoperation systems, as the sluggish dynamic responses of the master and slave manipulators tend to filter out the true environment impedance felt by the operator [8], [9]. Active control can only partially compensate for these shortcomings. Indeed, uncertainty in the open-loop frequency response of a given plant limits its achievable closed-loop frequency response (see, for example, [10]). Therefore, fundamental changes in the design of teleoperation systems are necessary.

The difficulties encountered in building sensitive multi-degree-of-freedom teleoperation masters have been discussed in [8], [11]. As suggested in [12], backdriveable multi-degree-of-freedom teleoperation masters with low mechanical impedance, high speed and accurate force exertion can be achieved by using parallel actuation. But the same type of parallel drive mechanisms could also be used as redundant fine-motion wrists mounted on robot arms, thus increasing the dexterity of the conventional manipulators presently used as teleoperation slaves. The advantages of such a coarse-fine approach to manipulation have been recognized before [13], [14], [15]. Devices with hydraulic actuation [14], two-dimensional flux-steering motors [16], conventional DC motors [17] and magnetic levitation [18], [15] have been developed and used before in coarse-fine systems.

A new teleoperation system based on parallel actuation and the coarse-fine approach to manipulation is presented in this paper. It is proposed that the teleoperation slave be a coarse-fine manipulator with a fine-motion wrist identical to the teleoperation master. As first suggested in [19], the fine motion technology chosen for this work is Lorentz magnetic levitation, introduced as the "Magic Wrist" in [20], [21], [15]. The wrist employed was designed and built at the University of British Columbia (UBC) along the principles described in [15]. Other fine motion devices, provided they have been designed to be backdriveable, to have low friction, no backlash, low impedance and high frequency response *i.e.*, to qualify as "sensitive" teleoperation masters [8], could have been used in a similar manner, but, as will be discussed in Section 5, Lorentz maglev devices are advantageous in many respects.

A Lorentz maglev wrist has been used before as a teleoperation master to control the motion of a scanning tunneling microscope [4] (although not in force-reflecting mode) and in a new "stiffness control" mode to control forces exerted by an excavator [22]. It has also been used in 6-DOF coordinated motion with a PUMA robot to demonstrate the feasibility of large-amplitude vibration isolation [23] and in coarse-fine assembly with a SCARA robot [24].

The issues of coordination, sensing and control that arise in the operation of the proposed force-reflecting teleoperation are also described in this paper. A wrist-level co-

S.E. Salcudean is with the Department of Electrical Engineering, University of British Columbia, Vancouver, BC, V6T 1Z4, Canada.

N.M. Wong was with the Department of Electrical Engineering, University of British Columbia, Vancouver, BC, V6T 1Z4, Canada. He is now with the Hong Kong TownGas Company

Ralph Hollis is with The Robotics Institute, Carnegie Mellon University, Pittsburgh, PA15213, USA

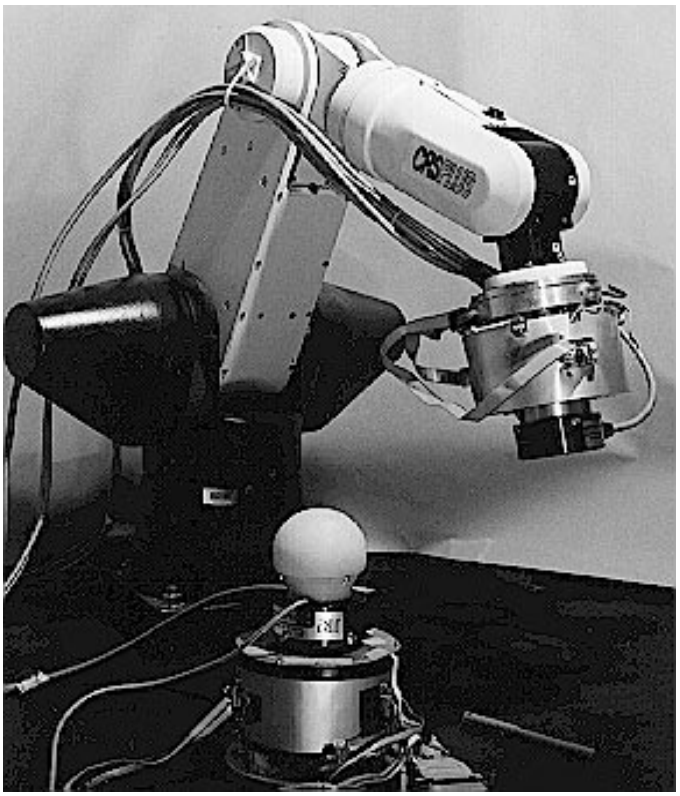

Fig. 1. Photograph of the UBC Teleoperation System.

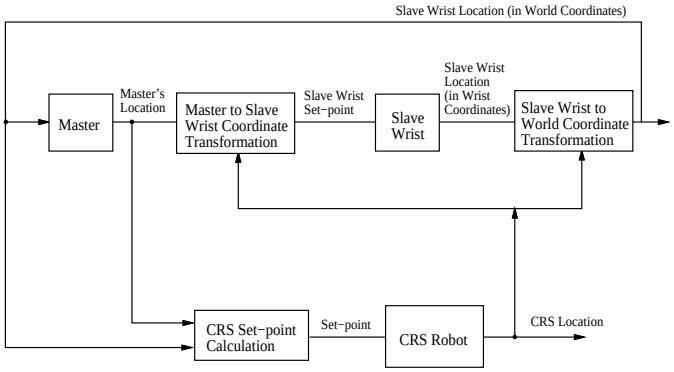

Fig. 2. Data-Flow of the UBC Teleoperation System

ordinated force approach emulating a massless rigid link between the master and the slave wrists is employed, as suggested in [25]. As done elsewhere [26], [27], feedforward of sensed hand forces to the slave and environment forces to the master is used to improve transparency. It is shown by simulations and experiments that such feedforward leads to poor stability margins in contact with stiff environments, unless substantial damping is added to the system. It is also shown by simulations and experiments that the coordination error can be substantially reduced by such sensed forces feedforward. If a simple adaptation of damping to sensed environment forces is applied, free-motion tracking performance and stiff-contact stability do not have to be traded against each other. This approach is similar to the estimated impedance feedback proposed in [28], but does not require environment identification.

Coarse positioning motion is achieved by using rate control to move the transport (coarse) robot in the direction pointed at by the master, whenever the teleoperation master is outside a pre-determined subset, or rate-control deadband, of its workspace. Experimental results show excellent system performance in free-motion tracking as well as in contact tasks.

The paper is organized as follows: In Section 2, the design of the UBC maglev wrist and of the UBC teleoperation system is described. In Section 3, issues of control and coordination of the teleoperation system described in Section 2 are discussed. Section 4 presents and discusses experimental results, Section 5 presents an evaluation of the UBC teleoperation system relative to surveyed performance specifications presented in the literature [11], [9], while Section 6 presents conclusions and suggestions for future work.

II. Teleoperation System Design

This section will describe the components of the UBC teleoperation system, as well as the computing subsystems and their interaction.

A photograph of the system can be seen in Figure 1. The slave manipulator is a conventional CRS A460 robot equipped with a maglev wrist. The master is a maglev wrist identical to the robot-mounted wrist. Each of the wrists is equipped with a JR^3 force-torque sensor, enabling measurements of operator hand forces at the master and environment forces at the slave.

The system data flow is illustrated in Figure 2. The CRS robot location (*i.e.*, position *and* orientation) reported by the robot is used to compute the relative locations of the two wrists, while the CRS robot set-point is determined from the master wrist location in a manner that will be described in Section 3.

A. UBC Maglev Wrist

An assembly sketch and a photograph of the UBC maglev wrist are shown in Figures 3 and 4, respectively. This wrist, designed by Salcudean according to the principles outlined in [21], [15], is an in-parallel actuated device in which six Lorentz forces are generated between two rigid elements - a stator and a "flotor". Only wires for power and sensor signals connect the two, the lighter flotor being actively levitated.

The maglev wrist has 120° symmetry. Three horizontal and three vertical flat coils are imbeded in the flotor. Each coil fits within the gap of a matching magnetic assembly attached to the stator. The flotor's horizontal plate has holes to allow supporting posts to hold the stator and the magnetic assemblies attached to it.

The UBC wrist fits within a cylinder with diameter of 132 mm and height of 110 mm. The stator mass is 2 Kg and the flotor mass is 0.65 Kg. The flotor has a motion range of roughly ± 4.5 mm in translation and $\pm 6°$ in rotation (from the nominal center, assuming that the translation and rotation are decoupled from each other, so the

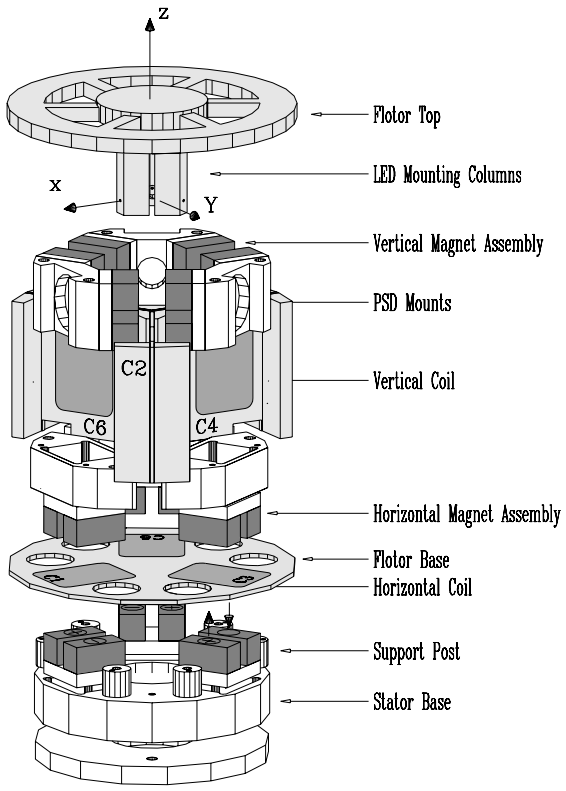

Fig. 3. The Assembly Sketch of the Maglev Wrist

numbers are somewhat optimistic). The magnetic gaps shown in Figure 3 are 11.5 mm, and the actuator magnets are 25×10×11.5 mm NdFeB 35 rectangular blocks (magnetized through the 11.5 mm side). The magnetic field in the magnetic gaps of the actuators exceeds 0.4 T. The coils, together with their protective covering, are 2.2 mm thick, and have time constants of the order of 0.1 milliseconds.

The UBC wrist optical position sensor is identical to the Magic Wrist's sensor [15]. It consists of three light-emitting diodes (LEDs), attached to the flotor, that project narrow, co-planar, infrared light beams at 120° from each other, onto the surfaces of three two-dimensional duo-lateral position sensitive diodes (PSDs). The positions of the beam projections onto the PSDs are detected and used to compute the location of the flotor with respect to the stator. The PSDs (with the 12-bit A/D conversion into the wrist controller) can detect flotor motion with a resolution of better than 5 μ m / 10 μ rad. The position sensor can be calibrated by driving the flotor to six mechanically stable positions and reading the sensor outputs at each of these positions.

A coordinate system can be attached to the intersection of the vertical coil axes (which coincides with the intersection of the LED light beams) of the flotor, and is defined as in Figure 3. Relative to this coordinate system, the wrench vector $w = [f_x\ f_y\ f_z\ \tau_x\ \tau_y\ \tau_z]^T$ acting on the flotor (at center position) when the flotor coils are energized

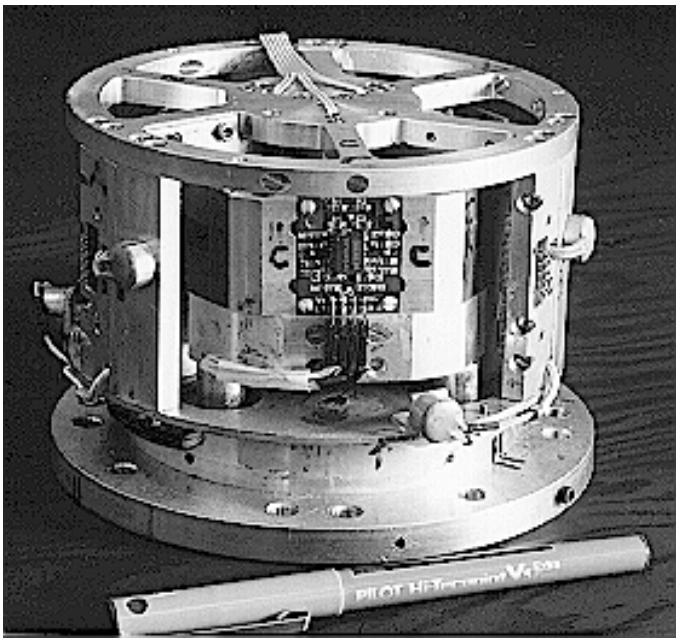

Fig. 4. UBC Maglev Wrist/Hand Controller

is given by $w = AI$, where $I = [I_1\ I_2\ ...\ I_6]^T$ is the vector of coil currents and A is the following transformation matrix:

$$A = \begin{bmatrix} 0 & 0 & -1.8 & 0 & 1.8 & 0 \\ 2.1 & 0 & -1.0 & 0 & -1.0 & 0 \\ 0 & 2.1 & 0.0 & 2.1 & 0 & 2.1 \\ 0.08 & 0.06 & -0.04 & 0 & -0.04 & -0.06 \\ 0 & -0.04 & 0.07 & 0.07 & -0.07 & -0.04 \\ 0.07 & 0 & 0.07 & 0 & 0.07 & 0 \end{bmatrix}. \quad (1)$$

The entries of the first three rows are in N/A, while those of the last three rows are in N-m/A, and were obtained by scaling the nominal values computed as in [15] by the measured actuator constant. From the singular value decomposition of A it can be seen that any force or torque direction can be generated without excessive coil currents. Since the matrix A does not change much within the workspace of the flotor, the inverse of the nominal value (1) is precomputed and used to determine the coil currents necessary to achieve a given wrench vector. If necessary, an externally mounted force-torque sensor, as shown in Figure 4, can be used for actuator calibration *i.e.,* for direct measurement of the columns of A.

A block diagram describing each of the maglev wrist systems is shown in Figure 5. The power amplifiers driving the coils can generate 10 A at up to 20 V each, but due to thermal constraints, the wrist coils can only be driven in steady-state with up to 3 A each.

In designing the UBC maglev wrist, the major goal was to minimize size without compromising performance. The Magic Wrist presented in [15] and the maglev wrist presented in [24] use coils arranged on the faces of a hexagonal cylindrical shell, thus leaving a center volume unused.

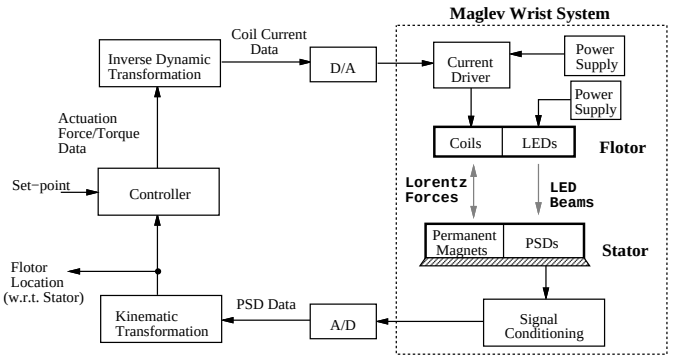

Fig. 5. Maglev Wrist System

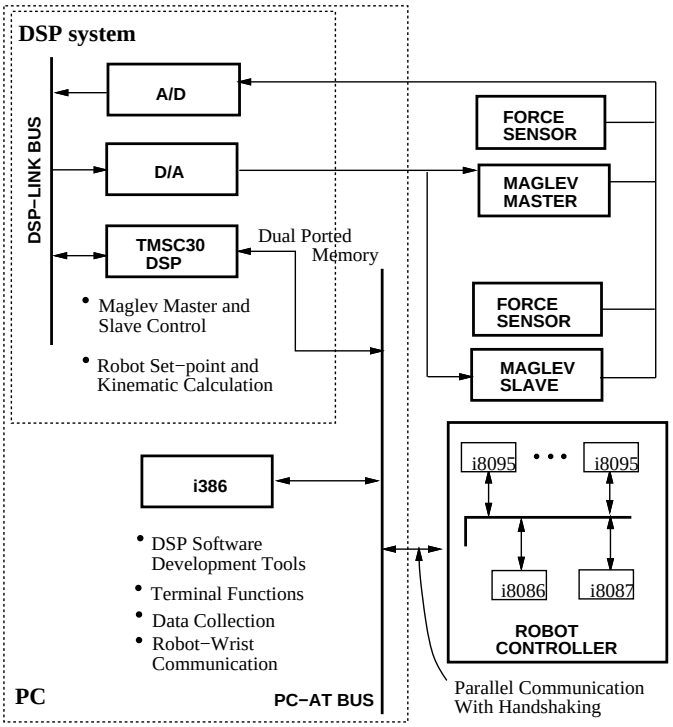

Fig. 6. The Real-Time Computing System

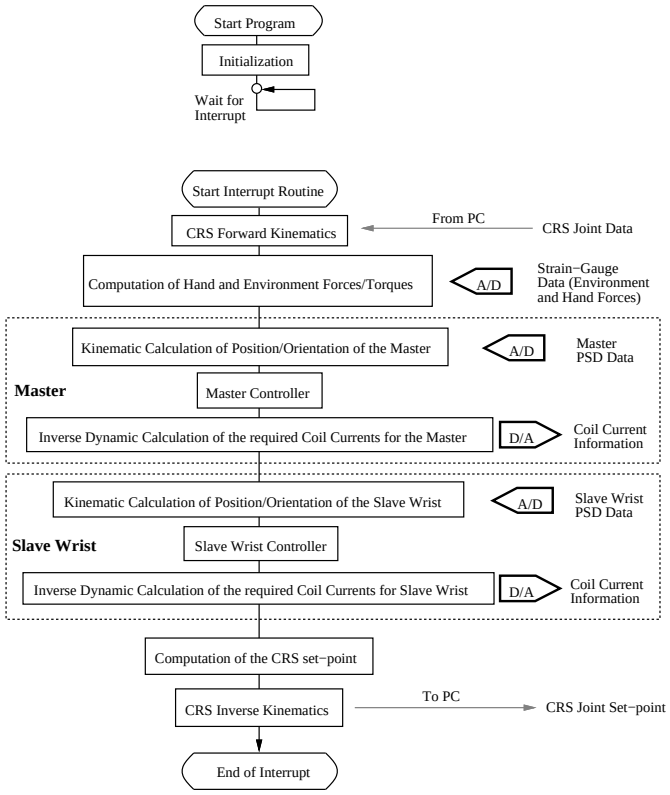

Fig. 7. Computations Performed by the DSP System

By using a star configuration, the UBC wrist becomes substantially smaller than both, although it can produce the same forces and only slightly reduced torques. The reason for minimizing size was the intended use of the device both as a fine-motion wrist, as suggested in [21] and as a teleoperation master, as suggested in [19].

B. Coarse Motion Manipulator

The coarse manipulator used in the UBC teleoperation system is an inexpensive, off-the-shelf CRS A460 robot. This robot is an elbow manipulator with an orthogonal spherical wrist and is powered by DC servo motors with timing belt and/or harmonic drive transmissions, depending on the joint.

From Figure 2, it is clear that the robot trajectory must be modified, in cartesian space, by the the external computer controlling the maglev wrists. In addition, the location of the robot must be reported to the maglev wrists controllers, so that the master and slave position and forces can be coordinated. These tasks must be accomplished as fast as possible.

The robot controller can communicate with the outside world through its serial port and through a 32-channel digital I/O port. Serial communication with the CRS robot has proven to be very slow. Indeed, it takes 42 ms to receive and send six (32-bit) floating point numbers, the minimum needed to report the CRS robot location to the teleoperation system controller and to transmit a new desired robot location. The delay is due mainly to the substantial communication protocol overhead. Parallel digital I/O communications to and from the robot can be done at a substantially faster rate. Indeed, it takes less than 2.8 ms to receive six 6-bit set-point increments and to transmit six 14-bit robot location data to a PC-based parallel I/O board.

A CRS robot state called REMOTE can be used for external computer control of the robot motion. Similar to the remote ALTER command of PUMA robots, REMOTE places the robot controller into a mode in which it expects position set-points to be delivered by an external computing system. Under this mode the CRS controller reads and updates the new set-point value from an internal data buffer at a fixed REMOTE loop clock rate. The REMOTE set-point can be specified in cartesian or joint coordinates, and in either absolute or incremental values. The incremental mode was selected because it is inherently safer and requires less data transmission.

When cartesian coordinates are specified to the remote

command, the CRS controller has to perform the inverse kinematics required to generate joint angle set points. In addition, if a cartesian position is to be reported by the CRS robot, the CRS controller has to perform the direct kinematics necessary to obtain gripper location from joint angles. Due to the relatively slow CRS control microprocessor (Intel 8086), the fastest REMOTE cartesian location set-point reception and cartesian location reporting cycle achievable was benchmarked at 55 ms, which includes the robot forward and inverse kinematics. This is slow, even when compared against other conventional robots. For instance, a PUMA 500 robot programmed in external ALTER mode can perform a similar task in 28 ms, using serial port communications [23].

C. Computing System

The real-time system employed for the coordinated control of the CRS robot, the maglev master and the maglev slave is illustrated in Figure 6. An IBM PC-AT compatible computer hosts a Spectrum Inc. DSP system, consisting of a system board using a Texas Instruments Inc. floating-point TMSC30 DSP chip and two analog input and output boards, all connected through a fast, private bus (DSP-LINK) that avoids the PC bus bottleneck. The PC communicates with the DSP system board via dual-ported memory mail-boxes and communicates with the CRS robot controller via a parallel I/O board. The floating point DSP board does most of the control and coordination work, by performing the tasks listed in Figure 7.

To gain flexibility and speed, the basic functions of A/D conversion, cross coupling removal, unit scaling and offset weight removal were moved from the JR^3 sensor support system to the DSP board. Thus the DSP system also computes the forces and torques from strain-gauge readings.

For the same reasons, the CRS robot's direct and inverse kinematic calculations that are required for the control of the system were re-written and moved from the CRS robot controller to the much faster DSP board. Through forward kinematic transformation of the reported CRS joint data, the robot gripper location is computed first, so that the slave flotor location and environment force data can be appropriately transformed. The CRS set-point is computed as a function of the master flotor location and is then expressed in joint space through the CRS inverse kinematics. Using joint-coordinate set-points, the fastest REMOTE clock rate achievable was improved from 55 ms to 16ms.

The DSP system takes about 5 ms to complete the CRS robot set-point, forward and inverse kinematics computations. However, these computations are only required every 16ms (*i.e.*, the maximum REMOTE rate), when the DSP controller finds new robot location data deposited by the PC in its mailbox. Without performing the CRS kinematics, the DSP system can complete force sensing and master and slave wrist controls within 2 ms, so the maglev wrist control update rate is roughly 500 Hz most of the time. Since the force bandwidth of the wrist mechanical system can be up to several kHz, the overall (wrist level) force bandwidth is limited by the computational delay.

The longer wrist control period (7 ms instead of 2 ms) that takes place when the CRS robot location is updated (every 16 ms or so) had no noticeable effect on the performance of the controller (the control gains are normalized to correspond to the same continuous time control gain). If this does turn out to become a problem in future work, it can be easily taken care of by increasing the interrupt cycle and executing the CRS kinematics routines in the main program (instead of waiting for the interrupt - see Figure 7).

III. Motion Coordination and Control

Most telemanipulation tasks consist of a coarse, free-motion, positioning phase followed by a small-motion contact phase. Therefore, two separate issues must be dealt with. The first one, which will be referred to as "motion coordination", is concerned with how to position the slave manipulator[1] within its workspace, given the small master workspace and the redundant coarse-fine structure of the slave. The second one involves dynamic modelling and bilateral control for transparency.

The issue of motion coordination will be treated essentially as the kinematic problem of generating slave manipulator set points from the master position. Control for transparency for small, wrist-level motions will be addressed in some detail. During rate control, the position of the master is integrated to generate a slave set-point. The effect of this integration on transparency during rate control with force feedback will only be touched upon, as this is still an open research problem.

A. Motion Coordination

By acting as a transporter, the CRS robot enlarges the workspace of the slave wrist by two orders of magnitude. The situation in which the slave manipulator workspace is much larger than that of the master, occurs naturally in teleoperation tasks, and is due to the fixed operator location and the limited operator hand motion range.

The most straightforward way of controlling a large workspace slave manipulator with a small workspace master is position control with scaling. Although this method preserves spatial correspondence, it suffers from poor control resolution. Indeed, in the system described in this paper, the sensing resolution of the master (5 μm) would correspond to 1 mm robot motion!

A solution to the position resolution problem caused by disparate workspace volumes of the master and slave is indexed position control [29]. By using an indexing switch, the master controls only a small portion of the slave workspace at a time. If the slave workspace far exceeds the master workspace, as is the case with the UBC teleoperation system, indexing would be required most of the time, and the operator would lose the sense of continuity during workspace switching. Furthermore, the addition of an indexing trigger makes single-handed control quite difficult.

[1] The redundant coarse-fine slave (robot with maglev wrist) will be referred to as the "slave manipulator".

The resolution and discontinuity problems associated with scaled position and indexed position control can be solved by using rate control, achieved by setting the slave velocity equal to the master position. However, because there is no direct position-to-position correspondence between master and slave, fine dextrous tasks are difficult to execute. This is described in [30], where it is shown that for small workspace telemanipulators, position control is superior for pick-and-place operations. The addition of force feedback is bound to make rate control performance relative to position control even worse. Indeed, it was found that force feedback in rate control mode creates an unnatural feel of the environment and has very poor stability margins. Under simplifying assumptions on the slave dynamics, it has been shown that an increase in the environment mass is perceived by the operator as an increase in environment viscosity, while an increase in environment viscosity is perceived as an increase in stiffness [31], [22]. Some of the "right feel" of position-to-position systems can be recovered in rate control by differentiating the signals returned to the master, but DC-signals, such as constant environment forces, would be lost in this process [31].

A.1 Hybrid Position and Rate Control

Since rate control can solve the resolution problem encountered in position control, while position control can solve the spatial correspondence and force feedback problems encountered with rate control, a new hybrid position/rate control approach is proposed. The approach consists of dividing the master workspace into a central region designated for position control, and a peripheral region designated for rate control. While the operator keeps the master within its position region (or rate deadband), the slave manipulator is controlled in position mode. When the operator hand pushes the master into the peripheral rate control region, the master position is integrated, thus moving the slave manipulator in rate control.

An easy way to interpret such a hybrid position/rate control approach is to imagine that the slave manipulator is controlled in position mode about a local (slave) frame. When the master is about to exceed its workspace, the center of the local frame is displaced or "dragged" towards the goal pointed at by the master. The proposed position/rate control scheme can be written as

$$\begin{aligned} X_{sd} &= c_p\, x_m + X_L \\ \dot{X}_L &= \begin{cases} f(\|x_m\|)\, x_m & \|x_m\| > r \\ 0 & \text{otherwise} \end{cases} \end{aligned} \tag{2}$$

where x_m, X_{sd} are the master and desired slave manipulator location, X_L is the slave manipulator local position control center, c_p is a position scaling factor, $f(\|x_m\|)$ is a positive increasing velocity scaling function and $\|\cdot\|$ is the max (or other) vector norm. The master position workspace $\{x_m : \|x_m\| \le r\}$ is mapped into a scaled local position workspace $\{X_{sd} : \|X_{sd} - X_L\| \le c_p r\}$ about X_L. The center X_L of the workspace can be moved in the intuitively simple way of pointing towards the desired center which triggers the rate control action. This approach can be thought of as position control with automatic indexing.

Closer examination reveals a problem with the hybrid position/rate control proposed above. Suppose that the slave robot is at a position $X_{sd} = X_0$ and the operator wants to reach a position $X_{sd} = X_1$ against a stiff wall, with $\|X_1 - X_0\| > c_p r$. The operator has to move the slave local frame since the goal is not within the position workspace of the slave and does so by moving the master outside its position workspace. By pointing the master precisely along $X_1 - X_0$, the operator takes the slave local frame into $X_1 - (c_p\|x_m\|/\|X_1 - X_0\|)(X_1 - X_0)$, where the motion has to stop, due to the wall constraint (note that $\|x_m\| > r$). So, at contact, the operator stops the slave manipulator by pulling the master back, *i.e.*, by bringing the master back into its position control region (note that, in the presence of force-feedback, the master will indeed be pushed back to its position control workspace by the stiff wall). As soon as the master enters its position control region, the slave manipulator tracks it and pulls away from X_1, which cannot be reached in position mode. The sequence can be repeated *ad infinitum* without ever being able to reach the goal.

There are two alternative solutions that deal with this problem.

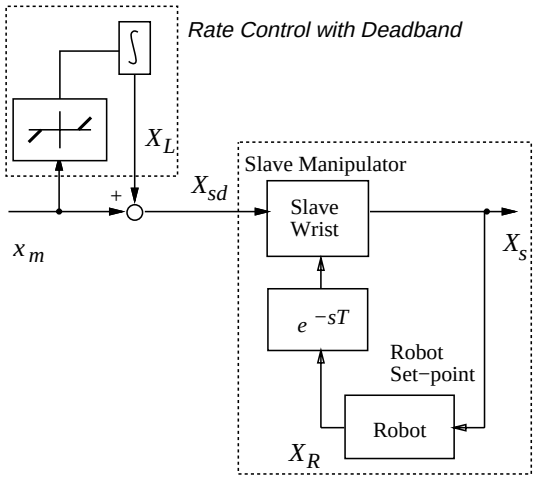

Fig. 8. Implementation of the Hybrid Position and Rate Control (small centering motion not shown).

The first is to stop the overall slave motion whenever the master is moved from the rate control zone to the position control zone and resume position control only when the master is nearly centered. In order to maintain the position correspondence between the master and the slave local positions (otherwise the slave will suddenly jump when position control is resumed), the local frame X_L should track the master reverse motion before the position control is reactivated. The loss of control over the slave manipulator while the master is centered is dangerous in contact tasks and leads to a loss of continuity in guarded moves and a loss of spatial correspondence.

The second solution to this "reachability" problem consists of adding a small "centering" motion so that the lo-

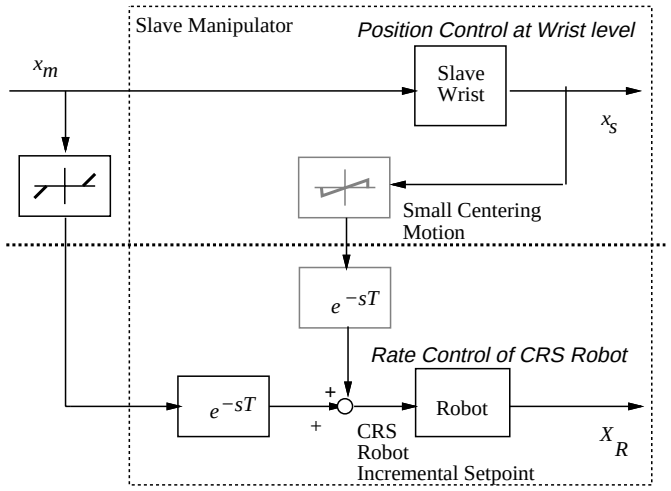

Fig. 9. Decoupled Coarse-Fine Control

cal slave frame *slowly* tracks the slave manipulator position when the master is in the position control workspace. This amounts to the addition of a small rate control term throughout the master workspace and modifies (2) to

$$\begin{aligned} X_{sd} &= c_p\, x_m + X_L \\ \dot{X}_L &= \begin{cases} f(\|x_m\|)\, x_m & \|x_m\| > r \\ c_v\, x_s & \text{otherwise,} \end{cases} \end{aligned} \tag{3}$$

where c_v is a small velocity scaling constant and $x_s = X_s - X_L$ is the "local" displacement of the slave.

Consider again the situation in which the slave manipulator has to be brought in contact with a surface. As before, when the slave reaches the goal and has to be stopped, the master is brought back into the position workspace and pulls the slave away from its goal. However, further pointing towards the surface slowly brings the slave in contact, as desired. The rate constant c_v in (3) of the local frame motion can be made small enough so as not to interfere with or even be noticeable by the operator.

The hybrid position and rate control described above was implemented on the UBC teleoperation system. In the first attempt, the slave flotor was controlled as a rigid body in space, with the CRS robot programmed to track it. This is illustrated in Figure 8, where X_R is the absolute position of the CRS robot.

The slave flotor absolute set-point X_{sd} is computed from the local frame X_L and the master position x_m. This approach to the control of the coarse-fine manipulator was suggested in [15] and is attractive because it reduces the function of the coarse robot to that of enlarging the flotor actuator gaps. Unfortunately, it was found that this control method leads to substantial step response overshoot, so much so that positioning of the slave robot becomes an annoying and time-consuming task. Simulation studies of a representative single-axis coarse-fine robot model, as discussed in [32], isolated the problem to the delay required to communicate the robot position from the CRS controller to the wrist controller. As seen in Figure 8, the robot position is fed back to the slave wrist. A delay in X_R adds phase lag to this feedback loop and causes oscillatory behavior.

The continuous tracking approach to coarse-fine coordination has a safety problem as well. If, for any reason, the slave flotor lost power and fell against its mechanical stops, the transport robot would follow until it would reach (or, more likely, crash into) the boundary of its workspace. A much simpler solution is proposed next.

A.2 Decoupled Coarse-Fine Motion Coordination

Since the slave overshoot problem is due mainly to the delay in the transport robot position, it can be solved by controlling the robot and slave flotor independently. Such a decoupling of coarse and fine motions can be achieved by setting the master and slave flotors in kinematic correspondence relative to their stators, and by commanding the transport robot to track its wrist flotor only when the slave flotor is about to exceed its motion range. Although implemented and found to work well, the safety of this approach in case of slave wrist power failure or payload overload is also questionable.

A better approach is to decouple the coarse and fine motions of the slave manipulator by letting the local frame X_L be identical to the transport robot position X_R, while position control is carried out between the two wrists (relative to their stator centers) at a control rate that is not limited by the robot controller. This is implemented as follows:

$$x_{sd} = x_m \tag{4}$$

$$\dot{X}_{Rd} = \begin{cases} f(\|x_m\|)\, x_m & \|x_m\| > r \\ c_v\, x_s & \text{otherwise,} \end{cases} \tag{5}$$

where $x_s = X_s - X_R$ is the slave flotor position relative to the slave stator, x_{sd} is its set-point, X_{Rd} is the coarse robot set-point, and X_s is the slave robot absolute position. The delay in X_R no longer causes a problem. It only means that when the operator wants to perform a large move by switching to rate control, there will be an imperceptible delay before the transport robot moves.

Instead of the actual slave flotor center X_s, the robot now tracks the slave flotor set-point X_{sd} obtained directly from the master. Therefore, the response time and safety of the system are improved. If either the master or the slave wrist loses power, the operator can still control the robot. The only drawback of the method as presented, is that the position scaling c_p cannot be larger than 1, although modifications of the (4) that also move the coarse robot in position control might work (these have not been tried yet). Figure 9 shows the improved hybrid position and rate control for the decoupled coarse-fine system.

Although computationally demanding, the six-degree-of-freedom implementation of the motion coordination algorithm proposed above is straightforward and follows directly from Figure 2 and Figure 9. Euler quaternions are used to parametrize rotation. The only choice involved is the shape of the velocity deadband of the master, which should match the master workspace as closely as possible. Details can be found in [33].

B. Wrist-Level Control

Because of the high ratio of its harmonic drives, the CRS robot has a high mechanical impedance and can be assumed to be a pure position source. Therefore, the dynamic interaction between the robot and the wrist attached to it, due mainly to the flexible modes of the robot arm, can be neglected.

The flotors of the maglev wrists can be modelled as single rigid bodies. With the rotational dynamics described using Euler quaternions, the differential equations describing the flotor motion can be transformed to decoupled double-integrator form by either exact (similar to computed-torque) or small angle approximate linearization [15]. This linearization includes gravitational feedforward terms (flotor weight and gravity torque) and justifies the use of single-axis mass models for the master and slave flotors:

$$ms^2 x_m = f_h + f_m \quad (6)$$

$$ms^2 x_s + ms^2 X_R = f_e + f_s \ . \quad (7)$$

where m_m, m_s, x_m, x_s are the master and slave flotor masses and positions with respect to their stators, respectively, X_R is the robot position, f_m and f_s are the master and slave actuation forces, and f_h and f_e are the hand and environment forces. Laplace-transformed variables are used throughout.

It will be assumed first that the robot acceleration is negligible. This will be the case while the master is within its rate deadband. For simplicity of the presentation, it will also be assumed that $m_m = m_s = m$. This is also the case in the experimental results presented in Section 4.

The hand and environment forces can be thought as having active exogenous components f_h^e and f_e^e, respectively, and feedback components $-H(s)x_m$ and $-E(s)x_s$ dependent on the hand and environment impedances, respectively (see, for example [28], [34]):

$$ms^2 x_m = f_h^e - H(s)x_m + f_m \quad (8)$$

$$ms^2 x_s = f_e^e - E(s)x_s + f_s \ . \quad (9)$$

Direct operation of the slave flotor when handled directly by the operator would correspond to

$$ms^2 x_s + H(s)x_s + E(s)x_s = f_h^e + f_e^e \ . \quad (10)$$

The goal of the teleoperation controller is to provide *transparency*, *i.e.*, *stability* of the mapping from exogenous signals to positions and a *matching of the transfer functions* from f_h^e, f_e^e to x_m, x_s in (8,9) to that from f_h^e or f_e^e to x_s in (10), for all $H(s)$ and $E(s)$ encountered during direct operation. Precise definitions can be given for transparency in terms of worst-case transfer functions errors, but these are beyond the scope of this paper.

The case $H(s) = bs$, $E(s) = k$, *i.e.*, the case in which the environment acts like a spring with spring constant k and the hand acts like a damper with damping constant b, is illustrative and plausible. Indeed, in contact tasks against stiff environments, the hand must act like a damper, otherwise a hand-held tool would chatter.

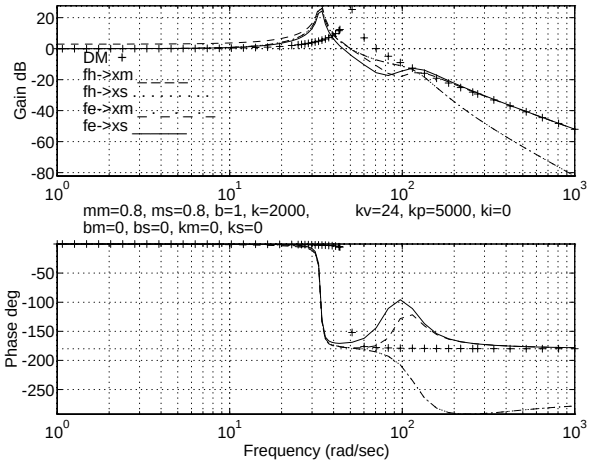

Fig. 10. Coordinated force controller against a compliant environment: *Magnitude Bode plots of the transfer functions ($f_h \to x_m$, $f_h \to x_s$, $f_e \to x_m$, $f_e \to x_s$) from hand and environment forces to master and slave positions are compared with the transfer function from hand or environment forces to the slave position in the case of direct manipulation (DM, denoted by +). The master and slave masses are 0.8 kg, and the environment stiffness $k = 2{,}000$ N/m and hand damping $b = 1$ N s/m are small by comparison to the coordinating torque controller gains k_p=5,000 N/m and k_v= 24 N s/m (no integral gain is used). For perfect transparency, all the plots should coincide with the DM plot. However, the coordinating torque controller effectively makes the master or slave feel like an object of twice the mass (note how the resonant peak is lowered in frequency).*

A bilateral controller based on a PID "coordinating torque" f_c can be implemented as follows [35]:

$$f_c = k_p(x_m - x_s) + sk_v(x_m - x_s) + \frac{1}{s}k_i(x_m - x_s) \quad (11)$$

$$f_s = f_c \quad (12)$$

$$f_m = -f_c \ . \quad (13)$$

A stiff rigid-link is emulated between master and slave by increasing k_p and k_v. As long as k_p and k_v are significantly larger than k and b, it can be shown that, although the coordinating torque controller does not provide transparency, it comes close, in the sense that the transfer function from external forces to master and slave positions emulate a mass-spring-damper system with the combined mass of the the master and slave. This is to be expected and is illustrated in Figure 10, which shows Bode plots from hand and environment stiffness to master and slave positions, as well as the "direct manipulation" transfer function.

If k_p and k_v are not very large, performance deteriorates, as the master position moves significantly more for the same applied force than it does in the case of direct manipulation. This is illustrated in Figure 11.

Because of the finite stiffness k_p, a position error $x_m - x_s$ is required to generate forces, causing a loss of kinematic correspondence between the master and the slave. When (stiff) force sensors are available, this major drawback of

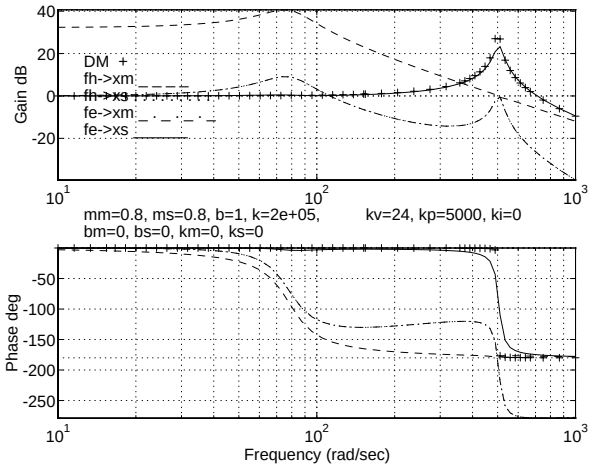

Fig. 11. Coordinated force controller against a stiff environment: *It can be seen that against a stiff environment (k = 200,000 N/m), the coordinating torque controller cannot prevent a loss of kinematic correspondence between the master and the slave, as the master moves much more in response to the hand force than the slave ($f_h \rightarrow x_m$ is much higher for teleoperation than it is for direct manipulation), while high frequency environment forces are filtered down at the master ($f_e \rightarrow x_m$ rolls off faster than for direct manipulation).*

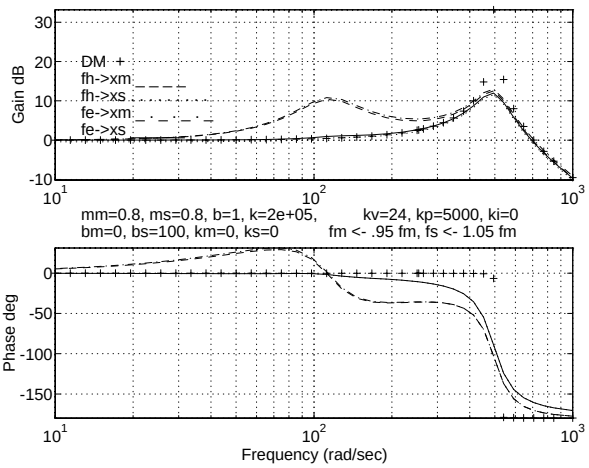

Fig. 12. Coordinated force control with force feedforward and damping against a stiff environment. *In the presence of even small errors (-5% for transmitted hand force and + 5% for transmitted environment force), substantial damping at the slave is required for a stable teleoperation system when a stiff environment is encountered. The teleoperation transfer functions are close to the direct manipulation transfer function at low and high frequency.*

the coordinating torque controller can be alleviated by feeding forward the measured hand and environment forces, given by $f_h = f_h^e - H(s)x_m$ and $f_e = f_e^e - E(s)x_s$, respectively:

$$f_c = k_p(x_m - x_s) + sk_v(x_m - x_s) + \frac{1}{s}k_i(x_m - x_s) \quad (14)$$

$$f_s = f_c + f_h \quad (15)$$

$$f_m = -f_c + f_e \ . \quad (16)$$

It is easy to show that the transfer functions from forces to the position error $x_m - x_s$ becomes zero, and that the transfer functions from forces to positions exactly match that of direct manipulation. The price one pays for such perfect transparency is lack of stability robustness to errors in force sensing, delays, etc., especially against stiff environments. Indeed, for the stiff environment of Figure 11, an error of only 5% in the forces fed forward drive the teleoperation system unstable. The sensitivity to modelling error and measurement noise can be reduced by additional damping at the slave (or master and slave) when the slave is in contact with the environment. This can be observed in Figure 12.

As seen in Figure 13, this additional damping causes a significantly lower frequency response relative to direct manipulation for soft environments or free motion. This will be felt at the master as in increase in environment viscosity. In order to avoid trading-off free-motion performance for stability during contact tasks, the amount of damping in the system can be adapted to the sensed environment force.

As an implementation detail, it should be noted that since it is awkward to allow the master and slave flotors to drift about when the operator does not hold the master, additional centering forces/torques should be added to f_s and f_m:

$$f_{s\_centering} = -k_s\, x_s - b_s\, sx_s \quad (17)$$

$$f_{m\_centering} = -k_m\, x_m - b_m\, sx_m \ ,$$

where k_m, b_m, k_s, b_s are small.

C. Force Feedback during Rate Control

The motion of the transport robot adds an inertial force to (8) during free motion, and an environment-dependent force during contact tasks.

Experimental results show that, during free motion, the additional inertial term can be felt mainly at switch-over points between position and rate control. This could cause "move-stop-move" oscillations on the rate control boundary. A control solution to this problem, possibly feedforward of inertial forces, is still being sought. Note that various scaling functions $f(x_m)$ in (4) (Figure 9 shows a piecewise linear function) including *smooth* ones, have been tried and found to have no noticeable effect.

In most contact tasks, the positioning robot is moving slowly and rate control does not affect reflected forces. However, it is clear that there are situations, such as dragging a brush while pressing down on the surface, in which there will be large-motion contact tasks. The above-mentioned problems with force-feedback during rate control have not yet been solved.

IV. Experimental Results

The control and motion coordination approaches described in the previous section were successfully implemented. The ability to easily position the slave flotor via

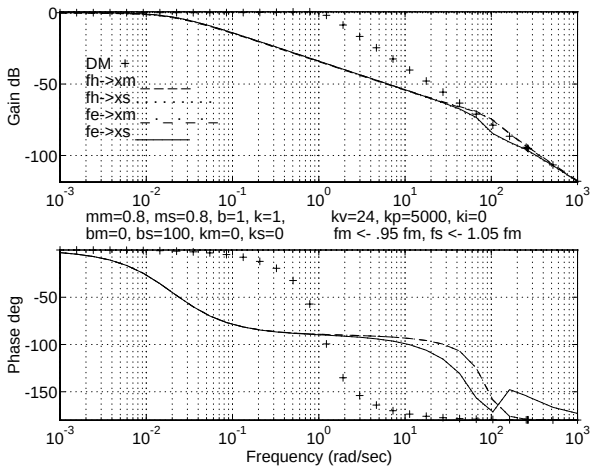

Fig. 13. Coordinated force with force feedforward controller against a compliant environment. *If the same high damping at the slave that is necessary to stabilize the teleoperation system against a stiff environment is used against a compliant environment, all forces to positions transfer functions roll off substantially faster than in the case of direct manipulation. This means that the system will feel sluggish to the operator and present high impedance to the environment.*

decoupled coarse-fine control was demonstrated. This was done by controlling the slave flotor with respect to the master stator, *i.e.*, with respect to a fixed coordinate system, as well as with respect to the slave wrist stator, *i.e.*, with respect to a moving coordinate system that roughly corresponds to "gripper frame". During hybrid position/rate control, a continuous beeping sound was implemented to indicate to the operator when the system is in rate mode. The most difficult aspect of slave robot positioning using the single-handed maglev master was found to be slave flotor orientation, which was found to take a bit of practice.

Two side-effects of force-feedback were noticed. The first one is the previously mentioned "move-stop-move" oscillation at the onset of rate control. This oscillation can be easily controlled by stiffening the grip on the handle. The second one is the high force feedback felt when hitting a hard surface while the robot is still moving. This effect has the rather fortunate consequence of pushing the operator's hand back into position mode, which in turn pulls back the slave wrist. This counteracts the robot motion, which cannot stop instantly, and is a helpful feature in avoiding damaging objects upon contact.

The kinesthetic feedback between master and slave has proven to be excellent. This has been tested by touching various surfaces and by using two operators, one manipulating the master, the other the slave.

The quantitative results that will be presented exhibit (i) free motion tracking in an unconstrained environment, (ii) contact with a constrained environment and (iii) exertion of forces on a constrained environment. The wrist level controllers used are the bilateral coordinated torque controller (11) and the bilateral coordinated force controller with force feedforward (14), both applied in the presence of small centering terms (17). Both wrists were equipped with the JR^3 force/torque sensors, even when the sensed force f_e and f_h were not used.

The gains of the above controllers were chosen as a compromise between transparency and stability margin and are shown in Table I.

TABLE I
CONTROLLER GAINS USED IN THE EXPERIMENTS REPORTED

Gains	Symbol	Value	unit
Proportional	k_p	5	N / mm
Velocity	k_v	0.024	N / (mm/s)
Integral	k_i	25*	N / (mm·s)
Centering spring	k_m, k_s	0.5	N / mm
Damping	b_m, b_s	0.005	N / (mm/s)

*There is a limit ($6 \times 10^{-3}\ mm \cdot s$) on the integrator term in order to prevent windup. Thus the integrator effect is never greater than 0.15N.

Unless specified otherwise, these gains are fixed, and the results presented are for the translational Z-axis. The characteristics for the other axes are similar and will not be shown here.

A. Bilateral Free Motion Tracking.

Wrist level position tracking is illustrated in Figure 14 and Figure 15. Figure 14 shows the master and slave wrist positions while the master wrist is driven by the operator and the coordinated force controller is applied. Figure 15 shows the master and slave wrist positions while the slave wrist is driven and the coordinated force with force feedforward is applied. Even at the highest frequency motion the operator hand could generate ($\simeq$ 7 Hz in these figures), the results show that the position tracking is very accurate, whether sensed forces are fed forward or not.

Figure 16 illustrates the hybrid position and rate control, with the master having a rate control deadband from -3 mm to +3 mm. The slave flotor position x_s with respect to its own stator tracks the master flotor at all times. While the operator moves the master flotor within the rate deadband (from $t = 0$ to $t = 2$ seconds), the robot motion is small and due only to the slow centering term in (17). While the master flotor is outside its position deadband, (from $t = 2$ to $t = 4$ seconds), the robot velocity tracks the master position. When the operator releases the master at $t = 4$ seconds, both the master and the slave flotors center themselves.

Backdriveability in rate mode is illustrated next, from $t = 5.2$ onwards, when the operator pulls the slave flotor back. The master tracks the slave flotor position and the robot tracks the master in rate control. Experiments show that the robot velocity tracks the master position up to frequencies of 2-3 Hz. Numerical differentiation of the robot position data adds to the velocity noise observed in Figure 16.

B. Stability in contact with stiff environment.

The master and slave positions and forces when the operator brings the slave in contact with a solid steel bar attached to the table are shown in Figures 17 (coordinated force control) and Figure 18 (coordinated force control with force feedforward). For coordinated force control, a loss of kinematic correspondence between master and slave can be seen, although force tracking is excellent. When the hand and environment forces are fed forward, the contact between the slave and the solid steer becomes unstable, unless the steer is held by hand (starting at $t = 5.2$ seconds), which provides additional damping.

By increasing the damping term, b_s from 0.005 to 0.1 N/(mm/s), the hard contact instability disappears, as illustrated in Figure VII. As described in the previous section, the trade-off is that the operator feels the master flotor drag during free motion (compare the hand force data in Figure 18 and Figure VII in the first few seconds of free motion).

A simple way in which the authors avoided the viscous drag felt during free motion was by adjusting the damping term according to the magnitude of the measured environment force. For instance, using

$$b_s = k_b \, |f_e| + b_{min}$$

with scaling $k_b = 0.01\,(mm/s)^{-1}$ and minimum damping $b_{min} = 0.0025N/(mm/s)$, there is no longer loss of stability when contacting a stiff environment. This is illustrated in Figure 20, when contact was made at $t \approx 3$ seconds, then a larger force was applied at $t \approx 5.5$ seconds.

C. Exertion of forces against stiff environment.

The results obtained with the coordinated force controller are shown in Figure VII. The operator moves the slave in rate control until the slave flotor hits the environment. The collision force pushes the master back into its rate control deadband zone and the robot rate motion stops (except for the small centering motion tracking the slave flotor). After the contact, the operator attempted to exert constant forces of 5N, 10N and 15N (the sensed environment force was displayed on the PC monitor). Excellent force tracking is observed even though no force sensor is used in the controller. For high forces, the position error between master and slave builds up. As the operator intended to exert a higher force at $t = 12$ seconds, the master crosses the rate deadband ($\pm$3mm), the CRS robot moves towards the solid steer. A large feedback force is generated to move the master back to the rate deadband zone, following which the operator moves the robot away from the point of contact.

Figure 22 shows the results obtained with the coordinated force with force feedforward controller (the damping term b_s was 0.1 N/(mm/s) to maintain contact stability for this controller). Since the force sensor is used in this controller, there are no position errors needed to generate forces. The problem of deadband crossing encountered previously is eliminated and the operator has a better sense of the environment stiffness.

V. Performance Relative to General Teleoperator Specifications

In this section, the performance of the system presented is evaluated against general specifications for teleoperation system transparency described in a number of surveys (*e.g.,* [11], [9]):

- *Positional Bandwidth.* There is a consensus that for "transparency", master-to-slave/slave-to-master positional bandwidths of 10-15 Hz are required. The position response of each wrist system exceed 30 Hz for translation and 15 Hz for rotation (with amplitudes of the order of 2 mm).
- *Force Bandwidth.* Force bandwidth requirements are usually estimated to be between 500 Hz and 5 kHz. The force bandwidth of this system is limited by coil inductance to several kHz, by computation delays to a few hundred Hz (this number will increase with faster processors and A/D converters) and by structural resonances (not yet quantified).
- *Backdriveability.* Since both operator and environment interfaces are free rigid bodies, arbitrarily small forces can backdrive the system. The limits are entirely dependent on software.
- *Volume of Operation.* This depends on the application, but should be as large as possible. The slave workspace of the system presented is essentially that of the slave robot. The master workspace is rather small. The authors have shown that augmentation of position control with rate control works well for translational motion. For rotational motion, it was found that operators have more difficulty referencing the motion to a particular frame.

  However, if desired, the master volume can be increased by mounting the maglev hand-controller on a position-controlled coarse-motion platform, *e.g.,* an inexpensive Stewart platform.

  Scaling of the present maglev wrists is also possible, with the generated forces varying roughly linearly with the flotor weight.
- *Force Thresholds.* The minimum master (slave) force required to move the slave (master) is limited only by the dynamic range of the maglev wrists position and force sensors and coil driver electronics. These numbers are in the 10-12 bit range, which means that for most practical purposes, the force threshold is zero.
- *Backlash.* Backlash in the slave transport robot acts as a disturbance on the slave wrist stator position. However, during fine-motion manipulation, the transport robot moves very little, since only the small centering motion is in effect. Therefore the transport robot backlash is significantly reduced.

  Note that, because the Lorentz forces generated between stator and flotor are relatively insensitive functions of their relative position, the flotor forces generated by backlash depend mainly on the coordinating torque gains in (14) and the local centering gains (17). If these are small ((17) always are), the effect of backlash will also be small.

- *Gravitational Balance.* Counterbalancing the arm is not necessary since the robot tracking the slave flotor is controlled in position mode. The master and slave flotors use gravity feedforward to make them feel weightless.
- *Arm Deflection and Static Errors.* These depend on the CRS (or other transport robot carrying the maglev wrist).
- *Maximum Velocities, accelerations and force/load capability.* The UBC wrist cannot sustain indefinitely a load higher than 15-20 N, although, from the transformation matrix A and the specifications of the coil drivers, it results that transient forces larger than 40 N can be obtained. The torque capability exceeds 0.6 N-m for indefinite loads, and more than 1.2 N-m for transient loads. This is more than adequate for a hand controller (indeed, the numbers exceed those of the JPL master arm [36]). However, there are a number of applications that require substantially larger loads, for which the system described in this paper is not suitable.
- *Force and Position Gain Ratios.* These are software selectable and should be decided based on stability and performance considerations.

In addition, the UBC teleoperation system offers the obvious advantage of single-handed control, of being a *safe direct drive system* (emergency power shutoff will simply cause the slave flotor to fall against its stator, while the coarse-positioning robot will just lock in position) and of allowing software emulation of a variety of master devices, such as a 2-DOF joystick.

Other technologies for the design of teleoperation masters have been proposed. All but magnetic levitation have an inherent disadvantage in their high mechanical impedance and requirement for linkages or guides, and/or actuator force transmission systems. Lorentz magnetic levitation technology can be scaled easily and lends itself to miniaturization. A maglev slave for microsurgery experiments with a flotor weight of 30 grams and continuous payload of 90 grams was designed and built at UBC [37].

VI. Conclusions and Future Work

This paper has presented a new teleoperation system based on magnetic levitation using Lorentz forces. Issues of design, motion coordination and control were addressed, offering novel approaches in all these respects. Experimental results, both qualitative and quantitative, were also presented, and demonstrate excellent performance. The work described here has shown that the UBC teleoperation system and, in general, *wrist-level kinematic and dynamic equivalent teleoperation systems employing the maglev technology of* [21], [15], offer exceptional advantages. In-parallel actuated platform-based systems (of the Stewart platform type or others) appear to be the competing technology, although it is quite difficult to design frictionless long-stroke force actuators suitable for a force-reflecting Stewart platform.

An approach to the control of master-slave systems with small workspace masters was presented. By combining position and rate control, an intuitive automatic indexing procedure was developed, allowing single-handed six-degree-of-freedom positioning of the slave. Details of implementation for redundant coarse-fine slave robots were also presented.

In terms of bilateral control, feedforward of sensed hand and environment forces was proposed as a way to reduce the coordination errors between master and slave. It was also shown that both contact stability problems and free-motion drag can be avoided by applying additional environment-dependent damping at the slave. Although adaptation to environment and hand impedance has been suggested before in [28], the simple scheme presented here does not require an environment "impedance estimator".

Enhancement plans for the hardware system include the addition of a camera mounted on the robot end-effector, in order to provide a "bird's eye" view of the slave flotor and workpiece. The computational environment is now being replaced with a VME/VxWorks-based system with SPARCengines and an Intel 860-based DSP board. A similar system incorporating substantial motion scaling between master and slave is being developed for microsurgery applications.

The issue of force feedback during slave rate control requires further research. Extensions of the teleoperation control scheme presented in Section 4 to more general master and slave models are also being pursued along the lines presented in [38]. The parametrization of all stabilizing compensators and H^∞ and other optimization-based designs are being used. On-line identification of inertial parameters of the master and slave wrists and their use in control algorithms is now being studied.

VII. Acknowledgements

The first author wishes to acknowledge the support of the National Research and Engineering Research Council of Canada (NSERC) through grants EQP 0093285, OGP 0046734 and a UBC-NSERC equipment grant. Thanks are also due to D. Fletcher for machining the two maglev wrists described in this paper, to the summer students C.T. Chen, D. Goertz and N. Ho for programming and electronics work, and to Professor D. Cherchas for providing access to his laboratory in the initial stages of this work.

References

[1] J. Jenkins, "Space Telerobotics Systems: Applications and Concepts," in *Proc. Workshop on Space Telerobotics*, vol. 1, (JPL Publ. 87-13), pp. 129–134, 1987.

[2] R.D. Merritt, E. Jackson, and F. Trice, "Remote defueling system for a damaged nuclear reactor," tech. rep., International Submarine Engineering, Port Coquitlam, B.C., Canada, August 1987. Presented at the DREP/RRMC Military Robotic Application Workshop, August 1987.

[3] I.W. Hunter, S. Lafontaine, P.M.F. Nielsen, P.J. Hunter, and J.M. Hollerbach, "A microrobot for manipulation and dynamical testing of single living cells," in *Proc. IEEE Micro Electro Mechanical Systems*, (Salt Lake City), pp. 102–106, February 1989.

[4] R.L. Hollis, S.E. Salcudean, and D.W. Abraham, "Towards a tele-nanorobotic manipulation system with atomic scale force

feedback and motion resolution," in *Proc. 3rd IEEE Micro Electro Mechanical Systems*, (Napa Valley, CA), February 1990. 6 pages.

[5] P.D. Lawrence, B. Sauder, U. Wallersteiner, and J. Wilson, "Teleoperation of Forest Harvesting Machines," in *Robotics in Forestry*, (Vaudreuil, Quebec), pp. 36–39, September 1990.

[6] M. Ostoja-Starzewski and M. Skibniewski, "A Master-Slave Manipulator for Excavation and Construction Tasks," *Robotics*, vol. 4, no. 4, pp. 333–337, 1989.

[7] R. Langreth, "Smarter Shovel," *Popular Science*, vol. 240, no. 6, pp. 82–84, 108–109, 1992.

[8] J. Vertut and P. Coiffet, *Robot Technology, Vol. 3A: Teleoperations and Robotics: Evolution and Development*. Prentice-Hall Series on Robot Technology, Prentice-Hall, 1986.

[9] T. Brooks, "Telerobotic Response Requirements," tech. rep., STX/ROB/90-03, STX Robotics, 4400 Forbes Blvd., Lanham, MD 20706, March 1990.

[10] J.C. Doyle and G. Stein, "Multivariable feedback design: Concepts for a classical/modern synthesis," *IEEE Trans. on Automat. Contr.*, vol. AC-26, pp. 4–16, February 1981.

[11] P. Fischer, R. Daniel, and K.V.Siva, "Specification and Design of Input Devices for Teleoperation," in *Proc. IEEE Conference on Robotics and Automation*, pp. 540–545, May 1990.

[12] K.V. Siva, A.A. Dumbreck, P.A. Fischer, and E. Abel, "Development of General Purpose Hand Controller for Advanced Teleoperation," in *Proc. International Symposium on Teleoperation and Control*, pp. 277–290, 1988.

[13] R. H. Taylor, R. L. Hollis, and M. A. Lavin, "Precise manipulation with endpoint sensing," *IBM J. Res. Develop.*, vol. 2, pp. 363–376, July 1985.

[14] Andre Sharon and David Hardt, "Enhancement of robot accuracy using endpoint feedback and a macro-micro manipulator system," in *American Control Conference proceedings*, (San Diego, California), pp. 1836–1842, June 6-8 1984.

[15] R.L. Hollis, S.E. Salcudean, and P.A. Allan, "A Six Degree-of-Freedom Magnetically Levitated Variable Compliance Fine Motion Wrist: Design, Modelling and Control," *IEEE Transactions on Robotics and Automation*, vol. 7, pp. 320–332, June 1991.

[16] R. L. Hollis, "A planar xy robotic fine positioning device," in *Proc. IEEE Conf. on Robotics and Automation*, (St. Louis, Missouri), pp. 329–336, March 25-28 1985.

[17] H. Kazerooni and J. Guo, "Direct-drive active compliant end-effector (active rcc)," *IEEE Journal of Robotics and Automation*, vol. 4, pp. 324–333, June 1988.

[18] Toshiro Higuchi, Masahiro Tsuda, and Shigeki Fujiwara, "Magnetic supported intelligent hand for automated precise assembly," in *Proc. Intl. Conf. on Industrial Electronics, Control and Instrumentation, SPIE*, vol. 801, pp. 926–933, November 1987.

[19] S.E. Salcudean, "Control Issues for Coarse-Fine Manipulators with Magnetically Levitated Wrists," September 1989. NASA Intelligent Robotic Systems Workshop, Center for Intelligent Robotic Systems for Space Exploration, RPI, Troy, NY.

[20] R. L. Hollis, A. P. Allan, and S.E. Salcudean, "A six degree-of-freedom magnetically levitated variable compliance fine motion wrist," in *Robotics Research, Vol. 4* (R. Bolles and B. Roth, eds.), pp. 65–73, MIT Press, 1988. Presented at the 4th International Symposium on Robotics Research, Santa Cruz, CA., August, 1987.

[21] R. Hollis, "Magnetically levitated fine motion robot wrist with programmable compliance," October 1989. U.S. Patent number 4,874,998.

[22] N.R. Parker, S.E. Salcudean, and P.D. Lawrence, "Application of Force Feedback to Heavy Duty Hydraulic Machines," in *Proceedings of the IEEE International Conference on Robotics and Automation*, (Atlanta, USA), pp. 375–381, May 2-6, 1993.

[23] S.E. Salcudean, H. Davis, C.T. Chen, D.E. Goertz, and B. Tryggvason, "Coarse-Fine Residual Gravity Cancellation System with Magnetic Levitation," in *Proceedings of the IEEE International Conference on Robotics and Automation*, (Nice, France), pp. 1641–1647, May 10-15, 1992.

[24] S.-R. Oh, R.L. Hollis, and S.E. Salcudean, "Precision Assembly with A Magnetically Levitated Wrist," in *Proceedings of the IEEE International Conference on Robotics and Automation*, (Atlanta, USA), pp. 127–134, May 2-6, 1993.

[25] M. Handlykken and T. Turner, "Control System Analysis and Synthesis for a Six Degree-of-Freedom Universal Force Reflecting Hand Controller," in *Proc. 19th IEEE Conference of Decision and Control*, pp. 1197–1205, December 1980.

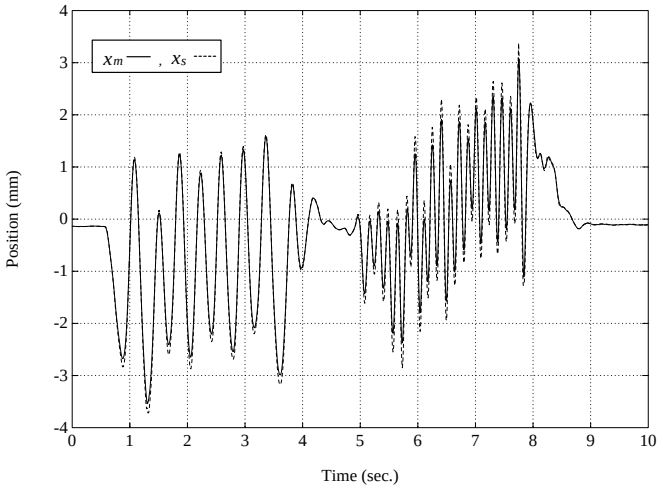

Fig. 14. Wrist-level free-motion tracking: coordinated force control is applied while the master is driven.

[26] D. A. Lawrence, "Designing Teleoperator Architecture for Transparency," in *Proceedings of the IEEE International Conference on Robotics and Automation*, (Nice, France), pp. 1406–1411, May 10-15 1992.

[27] Y. Yokokohji and T. Yoshikawa, "Bilateral Control of Master-Slave Manipulators for Ideal Kinesthetic Coupling," in *Proc. IEEE Conf. Robotics Automat.*, (Nice, France), pp. 849–858, May 10-15 1992.

[28] B. Hannaford, "A Design Framework for Teleoperators with Kinesthetic Feedback," *IEEE Transactions on Robotics and Automation*, vol. RA-5, pp. 426–434, August 1989.

[29] E.G. Johnsen and W.R. Corliss, *Human Factors Application in Teleoperator Design and Operation*. New York: Wiley-Interscience, 1971.

[30] W.S. Kim, F. Tendick, S.R. Ellis, and L.W. Stark, "A comparison of position and rate control for telemanipulations with consideration of manipulator system dynamics," *IEEE J. Robotics Automat.*, vol. RA-3, pp. 426–436, October 1987.

[31] N. Parker, "Application of force feedback to heavy duty hydraulic machines," Master's thesis, University of British Columbia, October 1992.

[32] S.E. Salcudean and C. An, "On the Control of Redundant Coarse-Fine Manipulators," in *Proceedings of the IEEE International Conference on Robotics and Automation*, (Scottsdale, Arizona), pp. 1843–1840, May 14-18, 1989.

[33] N.M. Wong, "Implementation of a force-reflecting telerobotic system with magnetically levitated master and wrist," Master's thesis, University of British Columbia, December 1992.

[34] H. Kazerooni, T.-I. Tsay, and K. Hollerbach, "A Controller Design Framework for Telerobotic Systems," *IEEE Transactions on Control Systems Technology*, vol. 1, pp. 50–62, March 1993.

[35] R.J. Anderson and M.W. Spong, "Bilateral control of operators with time delay," *IEEE Trans. Automat. Cont.*, vol. AC-34, pp. 494–501, May 1989.

[36] A. Bejczy and J. Salisbury, "Kinesthetic Coupling Between Operator and Remote Manipulator," in *International Computer Technology Conference, ASME Century 2 - Emerging Technologies*, pp. 197–211, 1980.

[37] S.E. Salcudean and J. Yan, "Towards a Motion Scaling System for Microsurgery," June 8-11 1993. The Third Annual IRIS-PRECARN Conference, Ottawa, Canada .

[38] S.E. Salcudean, N.M. Wong, and R.L. Hollis, "A Force-Reflecting Teleoperation System with Magnetically Levitated Master and Wrist," in *Proceedings of the IEEE International Conference on Robotics and Automation*, (Nice, France), pp. 1420–1426, May 10-15, 1992.

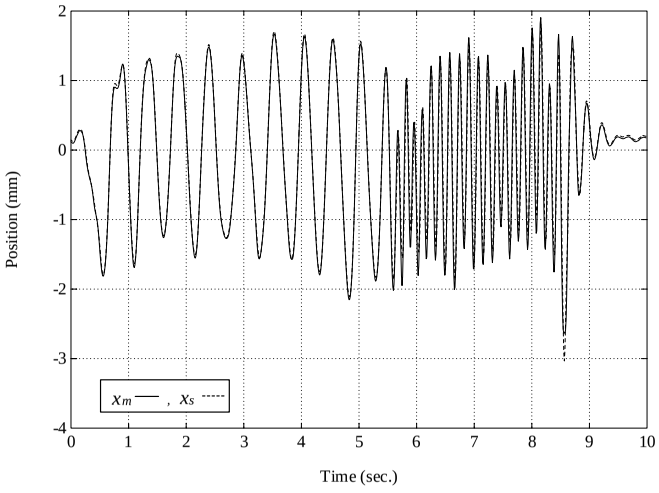

Fig. 15. Wrist-level free-motion tracking: the slave wrist is driven while coordinated force control with with hand and environment force feedforward are applied

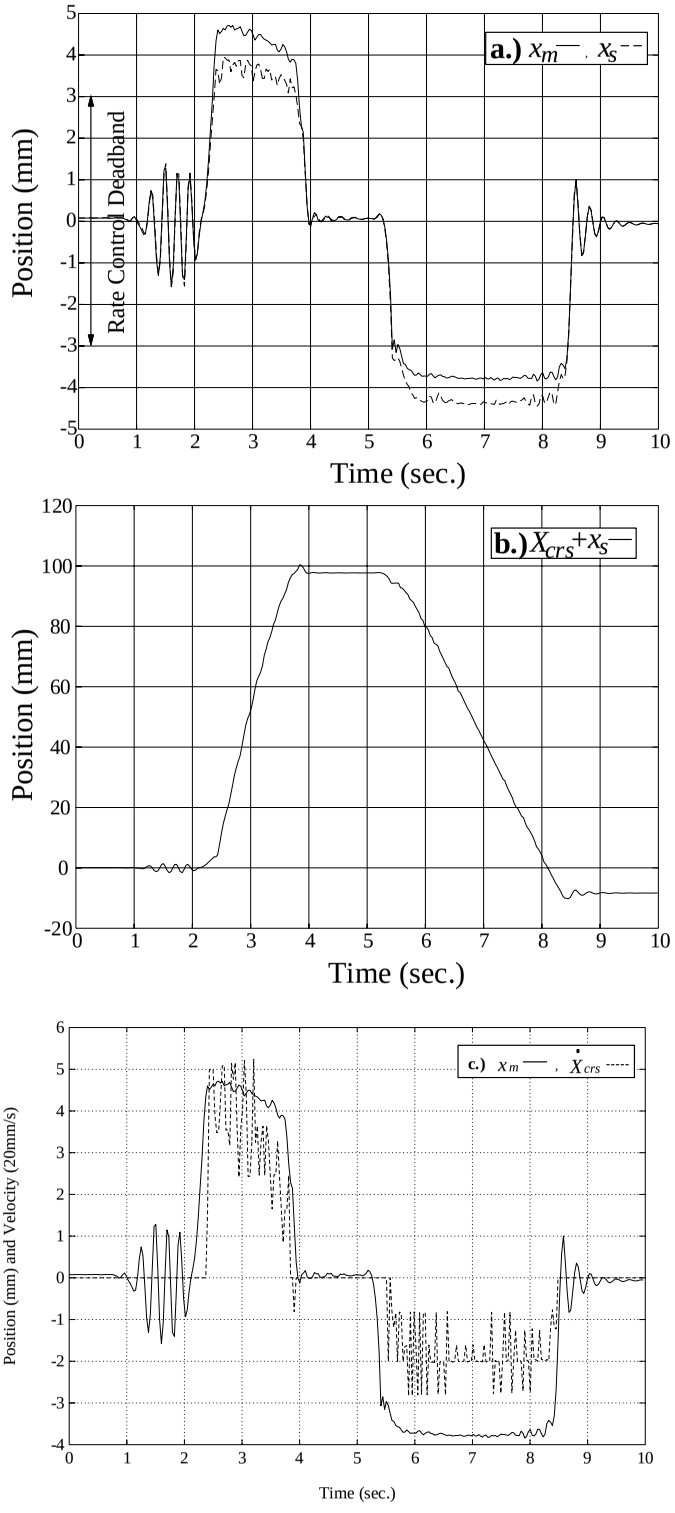

Fig. 16. Hybrid position/rate control: a.) Flotor position tracking: x_m and x_s; b.) Slave system motion: $X_R + x_s$; c.) Rate control: master position (x_m) and CRS robot velocity ($\dot{X}_{crs}$).

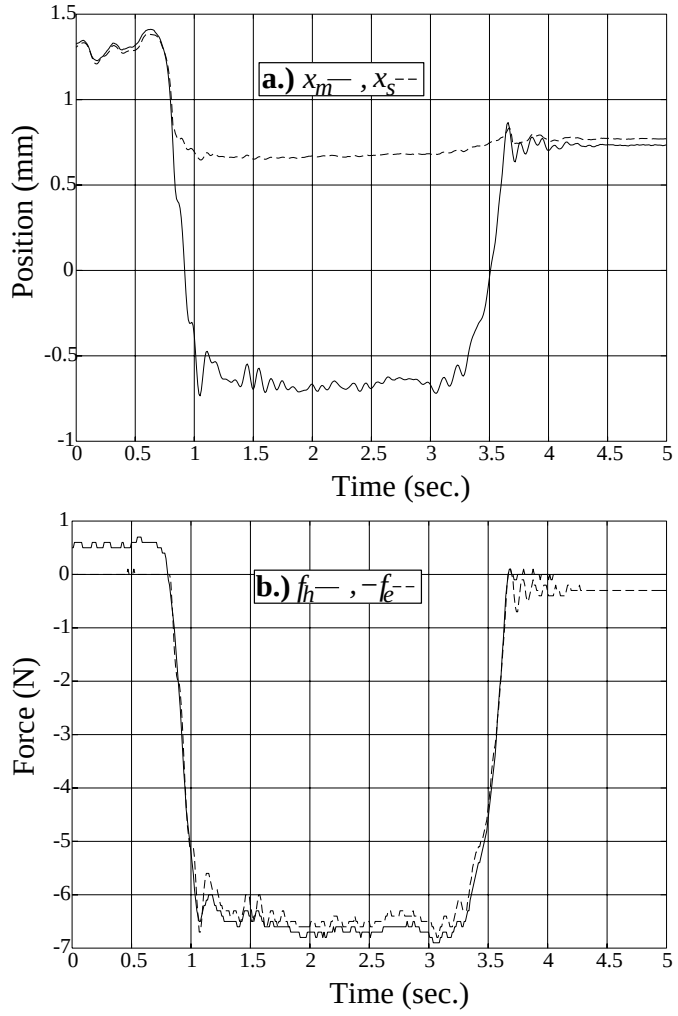

Fig. 17. Contact with stiff environment with coordinated force control: a.) master and slave flotor positions x_m and x_s; b.) hand and environment forces: f_h and $-f_e$.

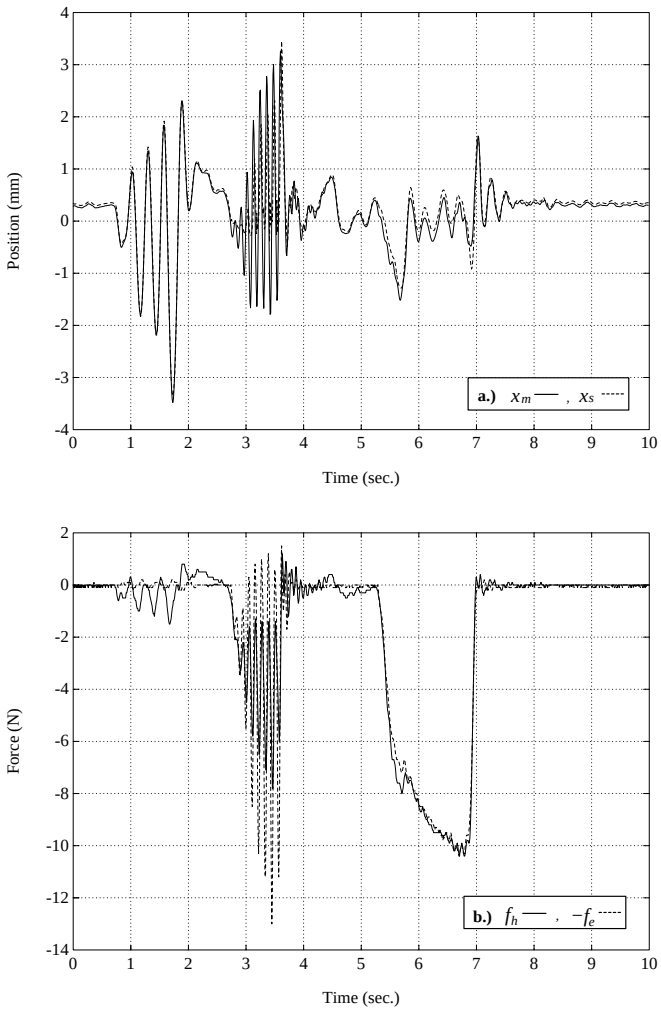

Fig. 18. Contact with stiff environment with coordinated force control and feedforward: a.) master and slave flotor positions x_m and x_s; b.) hand and environment forces: f_h and $-f_e$.

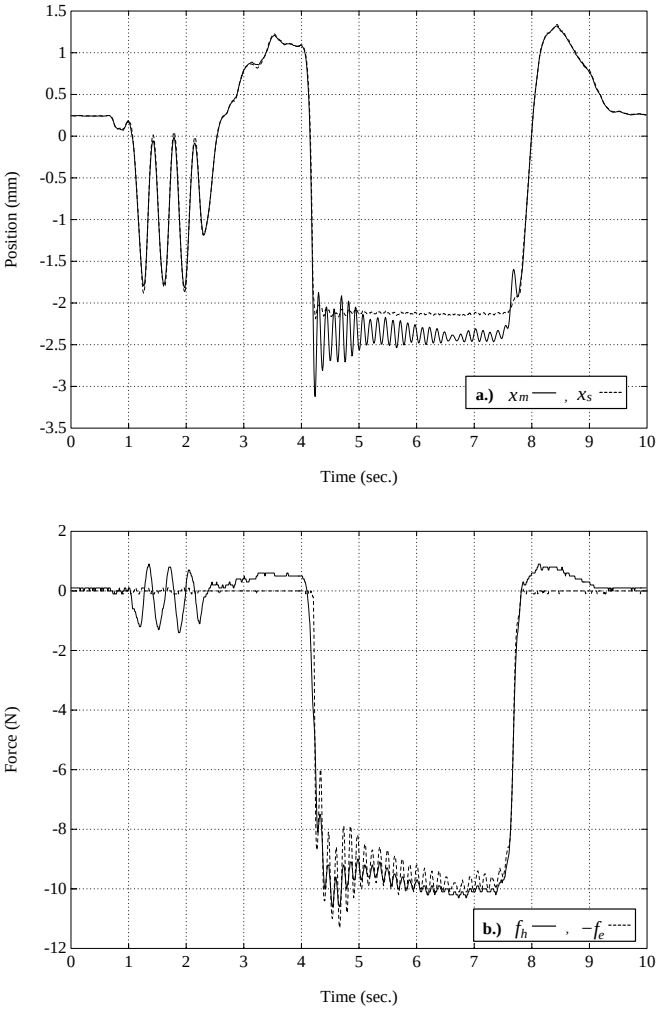

Fig. 19. Contact with stiff environment during coordinated control with force feedforward and large damping: a.) Master and slave flotor positions: x_m and x_s; b.) Hand and environment forces: f_h and $-f_e$.

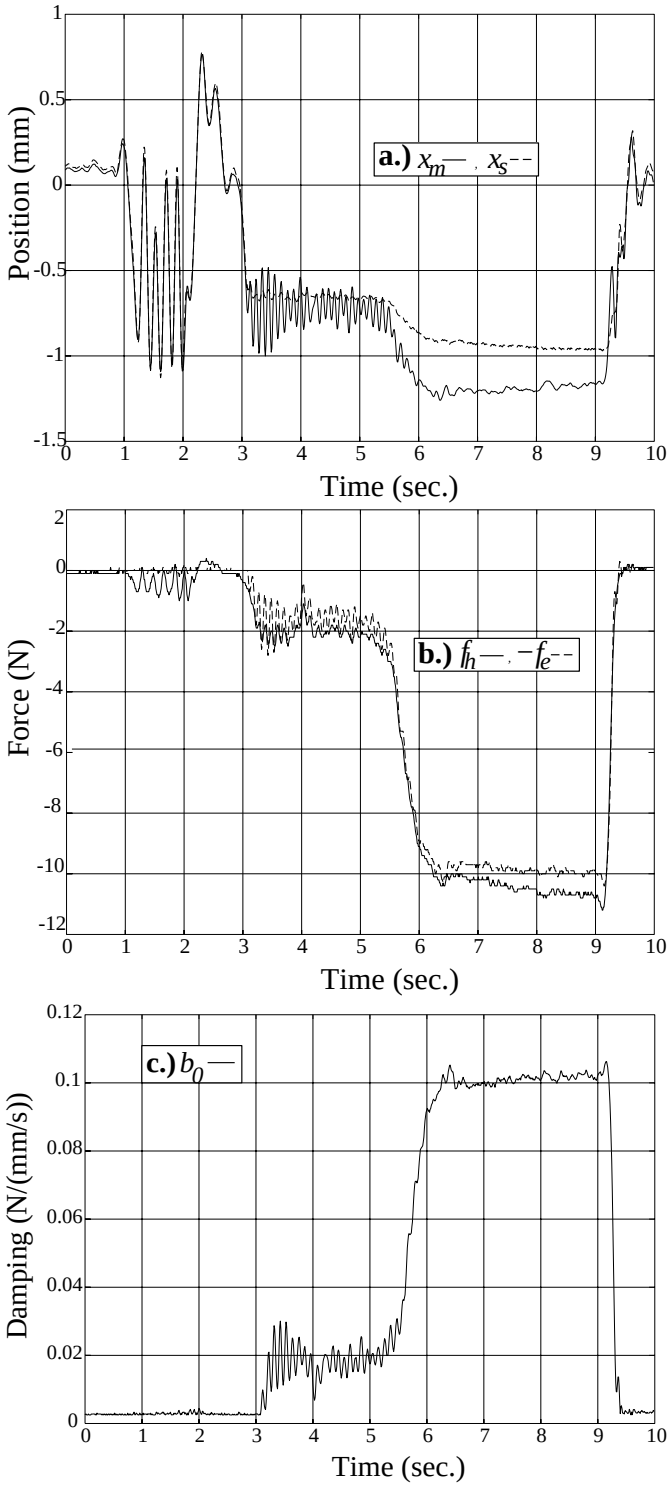

Fig. 20. Contact with stiff environment during coordinated force control with force feedforward and variable damping: a.) Master and slave wrist positions: x_m and x_s; b.) Hand and environment forces: f_h and $-f_e$; c.) Damping factor, b_0.

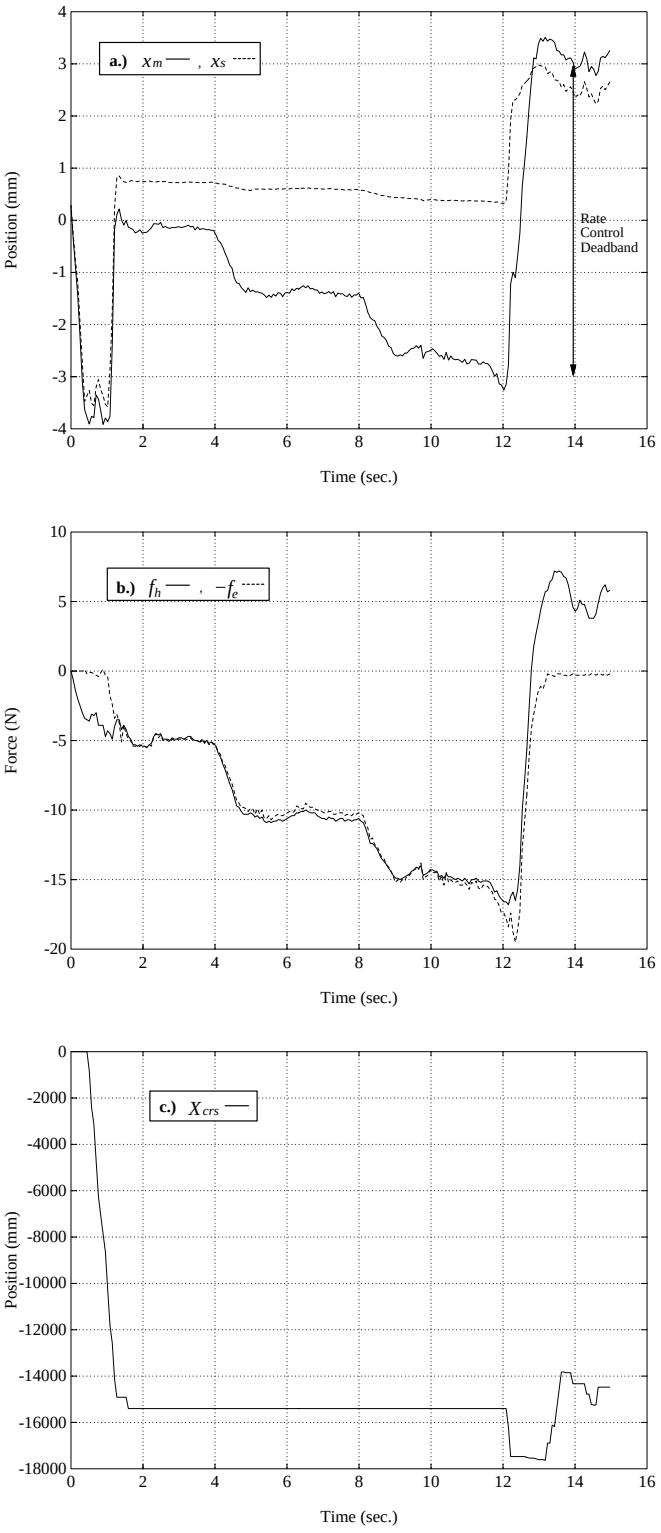

Fig. 21. Exertion of forces under coordinated force control. a.) Master and slave wrist positions: x_m and x_s; b.) Hand and environment forces: f_h and $-f_e$; c.) CRS robot motion: X_R.

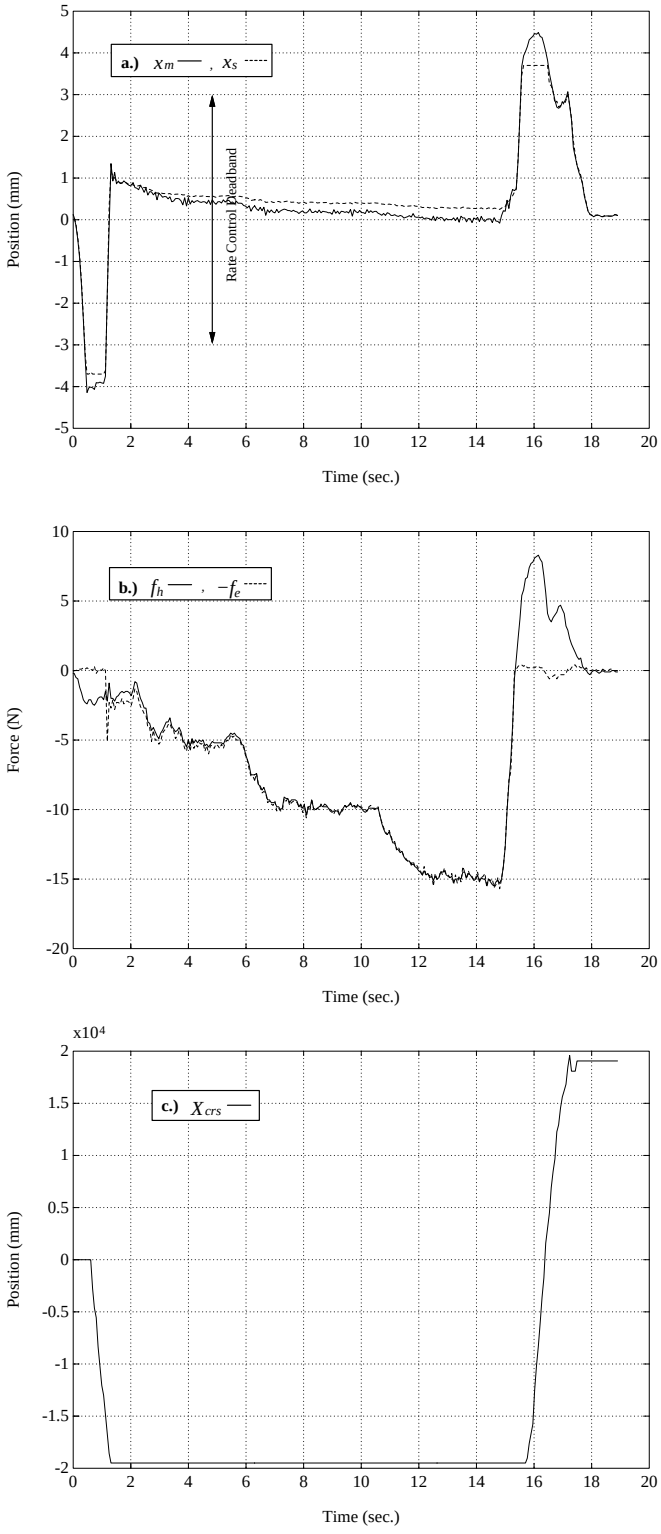

Fig. 22. Exertion of forces under coordinated force control with force feedforward. a.) Master and slave wrist positions: x_m and x_s; b.) Hand and environment forces: f_h and $-f_e$; c.) CRS robot motion: X_R.